

# PCCP

Accepted Manuscript



This is an *Accepted Manuscript*, which has been through the Royal Society of Chemistry peer review process and has been accepted for publication.

*Accepted Manuscripts* are published online shortly after acceptance, before technical editing, formatting and proof reading. Using this free service, authors can make their results available to the community, in citable form, before we publish the edited article. We will replace this *Accepted Manuscript* with the edited and formatted *Advance Article* as soon as it is available.

You can find more information about *Accepted Manuscripts* in the [Information for Authors](#).

Please note that technical editing may introduce minor changes to the text and/or graphics, which may alter content. The journal's standard [Terms & Conditions](#) and the [Ethical guidelines](#) still apply. In no event shall the Royal Society of Chemistry be held responsible for any errors or omissions in this *Accepted Manuscript* or any consequences arising from the use of any information it contains.



## Physical Chemistry Chemical Physics

## ARTICLE

## Perspectives on the energy landscape of Au-Cl binary system from the structural phase diagram of $\text{Au}_x\text{Cl}_y$ ( $x + y = 20$ )†

Zhimei Tian,<sup>a,b</sup> Longjiu Cheng<sup>a\*</sup>Received 00th January 20xx,  
Accepted 00th January 20xx

DOI: 10.1039/x0xx00000x

www.rsc.org/

Ligand-protected gold (Au-L) nanoclusters have attracted much attention, where the reported electronic and geometric structures show great diversity. To give a direct and overall view of the energy landscape of Au-L binary systems, the  $\text{Au}_x\text{Cl}_y$  ( $x + y = 20$ ) system is taken as a test case. By intensive global search of the potential energy surface at the level of density functional theory, a diverse set of global minimums and low-lying isomers are found at each composition, and the structural phase diagram is obtained. The unbiased global search is carried out using the method combining the genetic algorithm with TPSS functional. At  $x = 10$  with the stoichiometric ratio of Au and Cl (1:1), the cluster presents catenane structure. When  $x$  is in the range of 11-20, the clusters are Au-rich, and the Au-Cl system can be viewed as Cl-protected gold nanoclusters, where the gold cores consist of superatoms, superatom networks, or superatomic molecules in electronic structures. At  $x = 11-15$ , the gold cores consist of  $\text{Au}_3$ ,  $\text{Au}_4$  and  $\text{Au}_5$  2e-superatoms protected by staple motifs. At  $x = 16-20$ , the clusters are pyramidal superatomic molecules with one  $\text{Au}_{16}$  superatom core bonding with the four vertical atoms (Au or Cl). When  $x$  is in the scope of 9-5, the clusters are Cl-rich, and the 5d electrons of Au participate in bonding, resulting in high multiplicities. The Au-Cl binary system shows great diversity and flexibility in electronic and geometric structures, and there are corresponding structures to most of the experimentally produced Au-L nanoclusters in our structural phase diagram. We believe that the structural phase diagram gives an overall perspective to the universe of Au-L nanoclusters.

### I. Introduction

Gold nanoparticles of 2-3 nm bridge the “material gap”, which display distinct electronic transition in optical absorption, intrinsic magnetism, enhanced photoluminescence, and discontinuous charge transport and redox properties.<sup>1-4</sup> Due to the strong relativistic effects, gold atoms and clusters display many unique properties in chemical bonding. The interaction between gold and thiolate (SR), phosphine ( $\text{PR}_2$ ), and halogen (Cl) is of considerable importance in wide areas of modern science from both fundamental and practical viewpoints.<sup>5,6</sup> The ligand-protected gold Au-SR nanoclusters are of considerable importance for understanding of the structural evolution of clusters from small-to-medium sizes and relative stability of different optimized cluster geometries. Bare gold clusters in the size range  $n = 2-24$  have been well-studied, which undergo a series of structural transitions from planar, flat shell to cage, pyramid and to tubular motif.<sup>7-14</sup> For medium-sized gold clusters, the compact core/shell structures are likely a prevalent

structural form.<sup>15-19</sup> Ever since 2003, the  $\text{Au}_{20}$  cluster, which was first revealed by photoelectron spectroscopy, has received much attention.<sup>20-22</sup> The determination of the atomic structure at the nanoscale is a challenge. Experimentally, significant progress has been made in the chemical synthesis of ultrasmall ligand-protected Au nanoclusters. The first major breakthrough in total structure determination was achieved in 2007 by the Kornberg group, who determined the crystal structure of  $\text{Au}_{102}(\text{SR})_{44}$ .<sup>23</sup> Later, several clusters such as  $[\text{Au}_{25}(\text{SR})_{18}]^-$ ,<sup>24</sup>  $\text{Au}_{38}(\text{SR})_{24}$ ,<sup>25</sup>  $\text{Au}_{24}(\text{SR})_{20}$ ,<sup>26</sup>  $[\text{Au}_{20}(\text{PR}_2)_{10}\text{Cl}_4]\text{Cl}_2$ ,<sup>27</sup> and  $\text{Au}_{36}(\text{SR})_{24}$ ,<sup>28</sup> were experimentally determined. Structures of the experimentally synthesized ligand-protected gold (Au-L) nanoclusters can be well predicted by density functional theory (DFT) calculations and the success of DFT method in understanding and predicting the structures of Au-SR clusters are truly inspiring.<sup>29-31</sup>

The reported Au-L nanoclusters present various forms in electronic structures, including superatoms, superatom network, superatomic molecules, etc. To understand the intrinsic stability of Au-SR nanoclusters, Häkkinen and co-workers proposed the superatom complex concept based on the jellium model.<sup>32</sup> According to the concept, one determines the valence-electron count ( $V$ ) of the  $\text{Au}_m(\text{SR})_n^q$  cluster (where  $q$  is the charge of the cluster) by  $V = m - n - q$ . Each gold contributes one valence electron and each SR localizes one electron; if there are halogen groups in the cluster, each halogen also localizes one electron.<sup>33</sup> The appropriate aufbau rule of super shells for spherical Au

\*Email: clj@ustc.edu.

<sup>a</sup> Department of Chemistry, Anhui University, Hefei, Anhui, 230601, China.<sup>b</sup> School of Chemistry and Materials Engineering, Fuyang Teachers College, Fuyang, Anhui, 236037, China.

† Electronic Supplementary Information (ESI) available: The symmetries and relative energies of the low-lying isomers are given in Fig. S1 and Fig. S2, respectively. The superatomic models, AdNDP localized natural bonding orbitals of 17I, 18I and 19I clusters are collected in Figs. S3-S5. See DOI: 10.1039/x0xx00000x

## ARTICLE

## Physical Chemistry Chemical Physics

clusters is  $|1S^2|1P^6|1D^{10}|2S^2|1F^{14}|2P^6|1G^{18}|...$  (S–P–D–F–G–H– denote angular-momentum characters), associated with magic numbers 2, 8, 18, 34, 58, ...<sup>32</sup> Superatom theory has achieved great success in prediction of the stability of thiolate-protected gold nanoparticles, which can be understood by the magic numbers. Jiang et al. recently proposed  $[\text{Au}_{12}(\text{SR})_9]^+$ ,  $\text{Au}_8(\text{SR})_6$ ,  $\text{Au}_{10}(\text{SR})_8$  and  $\text{Au}_{15}(\text{SR})_{13}$  clusters for the magic number 2.<sup>34, 35</sup>  $[\text{Au}_{25}(\text{SR})_{18}]^-$  is associated with the magic number 8.<sup>24</sup>  $[\text{Au}_{44}(\text{SR})_{28}]^{2-}$  corresponds to the magic number 18.<sup>36</sup>  $\text{Au}_{102}(\text{SR})_{44}$  is associated with the magic number 58.<sup>37, 38</sup>

The superatom model can treat only those clusters with a spherical core, however, the stability of clusters with non-spherical cores cannot be understood. In addition, not all the Au-SR clusters exhibit magic numbers of free valence electrons as described by the spherical jellium model. According to the superatom model,  $\text{Au}_{38}(\text{SR})_{24}$  has 14 valence electrons and  $\text{Au}_{18}(\text{SR})_{14}$ ,  $\text{Au}_{20}(\text{SR})_{16}$  and  $\text{Au}_{24}(\text{SR})_{20}$  each has 4 valence electrons, both of which disagree with the count in the superatom model. Recently, Cheng and Yang proposed the superatom-network (SAN) model to explain the electronic stability of non-spherical shells of metal clusters.<sup>39</sup> The electronic stability of the 4e thiolate-protected nanoparticles  $\text{Au}_{18}(\text{SR})_{14}$ ,  $\text{Au}_{20}(\text{SR})_{16}$  and  $\text{Au}_{24}(\text{SR})_{20}$  follow the SAN model and the  $\text{Au}_8^{4+}$  core of the three clusters should be viewed as two non-conjugate 4-center 2-electron (4c-2e) tetrahedral  $\text{Au}_4$  superatoms.<sup>39</sup> The structure of  $\text{Au}_{44}(\text{SR})_{28}$  is theoretically predicted via DFT calculations and the  $\text{Au}_{26}^{(+10)}$  core can be viewed as a network of eight tetrahedron  $\text{Au}_4$  superatoms according to the SAN model.<sup>40</sup>

The super valence bond (SVB) model is another model proposed to explain the electronic stability of non-spherical shells of metal clusters.<sup>41</sup> The electronic shell of  $\text{Au}_{38}(\text{SR})_{24}$  has been studied, and the 23c-14e bi-icosahedral  $\text{Au}_{23}^{(+9)}$  core is proved to be a superatomic molecule.<sup>42</sup> A very recent study is carried out on  $\text{Au}_{20}$  pyramid following the SVB model, and its superatomic 16c-16e core is bonded with four vertical Au atoms.<sup>43</sup> The  $\text{Au}_{20}^{(+6)}$  core of  $[\text{Au}_{20}(\text{PPhy}_2)_{10}\text{Cl}_4]^{2+}$  nanocluster can be taken as a superatomic molecule bonded by two 11c-7e superatoms.<sup>44</sup> For the homoleptic  $[\text{Au}(\text{SR})_n]$  clusters with Au/SR ratio 1:1, there are no stacked Au core but exhibit only chain, ring, and catenane structures.<sup>45</sup>

As mentioned above, there have been a great number of studies on Au-L nanoclusters, which show great diversity on geometric and electronic properties resulting from the unique energy landscape (EL) of Au-L systems.<sup>24, 29, 46-53</sup> However, there still has no direct and overall study on the EL of Au-L systems. Using  $\text{Au}_x\text{Cl}_y$  binary system as a test case, we try to have a look at the EL of Au-L systems. Here we choose Cl representing L due to practical reason. Moreover, we select the size  $n = x + y = 20$ , where the two magic number clusters  $\text{Au}_{10}(\text{SR})_{10}$  and  $\text{Au}_{20}$  are contained.<sup>20, 45</sup> In previous reports, the EL of binary nanoalloy clusters at the same cluster size are studied.<sup>54</sup> The low-lying isomers of the Au-Cl nanoclusters and the structural phase diagram (SPD) are obtained, showing great diversity and flexibility of electronic structures.

## II. Computational Details

The global minimum search for the isomers of Au-Cl system is performed using genetic algorithm (GA) coupled with DFT, which has been successfully applied in the structural prediction of a number of systems.<sup>41, 55-58</sup> GA is a search heuristic that mimics the process of natural selection.<sup>59</sup> This heuristic is routinely used to generate useful solutions to optimization and search problems. GA belongs to the larger class of evolutionary algorithms, which generate solutions to optimization problems using techniques inspired by natural evolution, such as inheritance, mutation, selection, and crossover.<sup>60, 61</sup> DFT based GA is very time-consuming, and for each cluster, more than 1000 samplings are optimized by DFT. The quantum chemical calculations are carried out on the GAUSSIAN 09 suite of programs.<sup>62</sup> In the optimization procedure, the Def2-TZVP basis set is used for Au which obtains from the basis set exchange<sup>63, 64</sup> that accounts for scalar relativistic effects, and 6-311G\* basis set is used for Cl with generalized gradient approximation method by Tao-Perdew-Staroverov-Scuseria (GGA-TPSS)<sup>65</sup> without any symmetry constraint. The normal mode frequencies are also computed at the same level to ensure that they belong to real minima. The energies of the structures reported hereafter include the contribution of zero point energy (ZPE) corrections. For Au-Cl system at  $x \leq 9$ , the multiplicities are set to 1, 3, 5, 7 and 9 to find the most stable isomers. The natural bond orbital (NBO)<sup>66</sup> analyses are calculated using TPSS functional with Lan2dz basis set for Au and 6-31G\* basis set for Cl. To elucidate the nature of the chemical

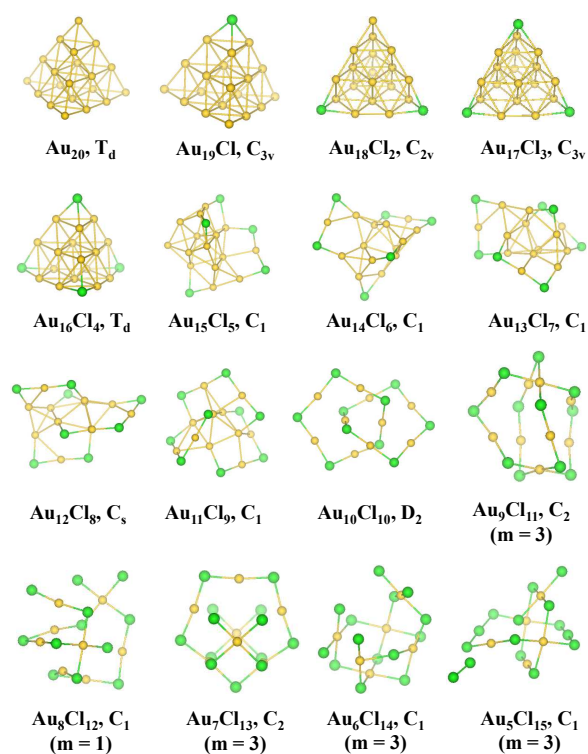


**Fig. 1** Lowest-energy structures of  $\text{Au}_x\text{Cl}_y$  ( $x + y = 20$ ) clusters optimized at TPSS/Def2-TZVP (Au) and 6-311G\* (Cl) level of theory. Au, yellow, Cl, green. At  $x \leq 9$ , enclosed are multiplicities of the molecules.

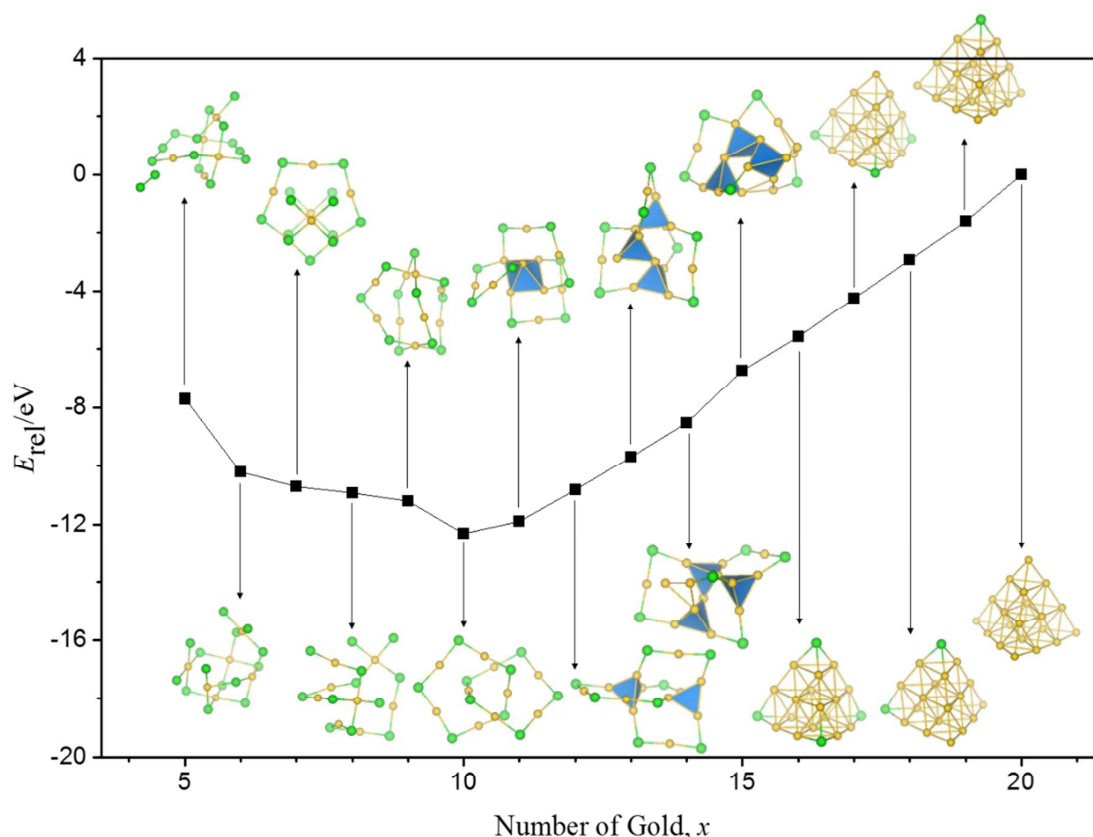


**Fig. 2** Lowest-energy structures of  $\text{Au}_x\text{Cl}_y$  ( $x + y = 20$ ) clusters optimized at TPSS/Def2-TZVP (Au) and 6-311G\* (Cl) level of theory. Au, yellow, Cl, green. The global minimum structures are also labeled, and the polyhedral models are used for  $\text{Au}_{11}\text{Cl}_9$ - $\text{Au}_{15}\text{Cl}_5$  clusters.

bonding, the adaptive natural density partitioning (AdNDP) is used to analyse the chemical bonding.<sup>67</sup> AdNDP is based on the concept of the electron pair as the main element of chemical bonding models, which recovers both Lewis bonding elements (1c-2e and 2c-2e objects) and delocalized bonding elements ( $nc-2e$ ). Molecular visualization is performed using MOLEKEL 5.4.<sup>68</sup>

### III. Results and Discussion

The lowest-lying equilibrium geometries and their symmetries of Au-Cl clusters are shown in Fig. 1, and the multiplicities of the Cl-rich clusters are also shown. Worth noting is that the structures of the Au-Cl clusters are broken up into pieces when  $x \leq 4$ , which are meaningless for the experiments in Au-L systems and are excluded in this work. We locate the global minimum structures and some relative stable isomers indexed in Roman numeral (such as I, II, III, ... for  $\text{Au}_{20}$  by the energy from low to high) in Fig. S1† and Fig. S2†.

#### 1. Structural Phase Diagram

To give a direct view of the structural evolution of the Au-Cl systems, Fig. 2 plots the structural phase diagram (SPD), a function of stability versus composition. The stability of  $\text{Au}_x\text{Cl}_y$  cluster is defined as the relative energy ( $E_{\text{rel}}$ ) taking  $\text{Au}_{20}$  and  $\text{Cl}_2$  as references. The calculated binding energy of  $\text{Cl}_2$  at the computational level in this work (2.23 eV) is in good agreement

with the experimental value (2.52 eV), indicating high reliability of the computational method.<sup>69</sup>

$E_{\text{rel}}$  is calculated according to the formula:

$$E_{\text{rel}} = E(\text{Au}_x\text{Cl}_y) - xE(\text{Au}_{20})/20 - yE(\text{Cl}_2)/2,$$

wherein  $E(\text{Au}_x\text{Cl}_y)$ ,  $E(\text{Au}_{20})$  and  $E(\text{Cl}_2)$  are the energies of  $\text{Au}_x\text{Cl}_y$ ,  $\text{Au}_{20}$  and  $\text{Cl}_2$ , respectively, including ZPE corrections. The magnitude of the absolute value of  $E_{\text{rel}}$  represents relative stability of the cluster. The more negative is  $E_{\text{rel}}$ , the more stable is a cluster. As shown in the figure, it is obvious that  $E_{\text{rel}}$  decreases as  $x$  varies from 5 to 10, and increases as  $x$  changes from 10 to 20. At  $x = 10$  with the stoichiometric ratio (1:1), the  $E_{\text{rel}}$  is the most negative (-12.32 eV), indicating the highest stability. There is a sudden increase of  $E_{\text{rel}}$  when  $x$  changes from 10 to 9, where the clusters become Cl-rich. This indicates that it is difficult to obtain Cl-rich clusters in contrast to the 1:1 Au-Cl cluster. There is another sudden increase at  $x = 5$ , which is perhaps due to the instability of  $\text{Au}_5\text{Cl}_{15}$  that contains a separate  $\text{Cl}_2$  molecule. Interestingly, the SPD curve at  $x = 10$ -20 is very smooth which indicates that the energy landscape of gold-rich Au-Cl clusters is very smooth and any ratio of Au and Cl is possible at certain experimental conditions.

#### 2. Geometric and electronic structures

When  $x = 10$ , the stoichiometric ratio of Au and Cl is 1:1, and it presents catenane structure. The canonical Cl-Au-Cl units emerge in the structure.  $\text{Au}_{10}\text{Cl}_{10}$  is in  $D_2$  symmetry, with

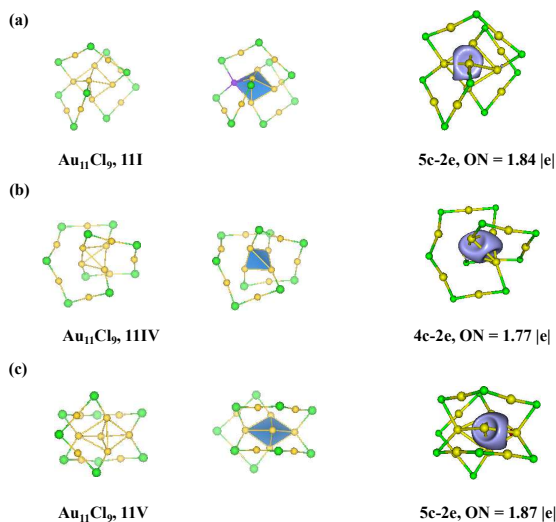


**Fig. 3** Structures, superatom models and AdNDP localized natural bonding orbitals of the three isomers of  $\text{Au}_{11}\text{Cl}_9$ : (a) 11I, (b) 11IV and (c) 11V. Au, yellow, Cl, green.

interlocked pentamer rings. This catenane-like structure is a unique feature of homoleptic  $[\text{Au}(\text{I})\text{-SR}]_n$  ( $n = 10-12$ ) complexes,<sup>7, 52</sup> and low Au/SR ratio Au-SR cluster, such as  $\text{Au}_{24}(\text{SR})_{20}$ .<sup>29, 70, 71</sup>

When  $x$  is in the range of 11-20, the clusters are Au-rich, and the Au-Cl clusters can be viewed as Cl-protected gold nanoclusters. When  $x$  is in the scope of 9-5, the clusters are Cl-rich and the  $5d$  electrons of Au atoms participate in bonding, resulting in high multiplicities.

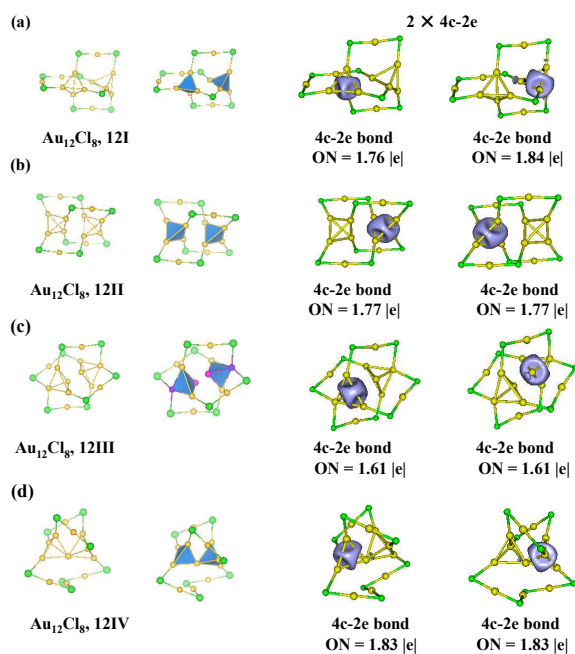


**Fig. 4** Structures, superatom-network models and AdNDP localized natural bonding orbitals of the four isomers of  $\text{Au}_{12}\text{Cl}_8$ : (a) 12I, (b) 12II, (c) 12III and (d) 12IV. Au, yellow, Cl, green.

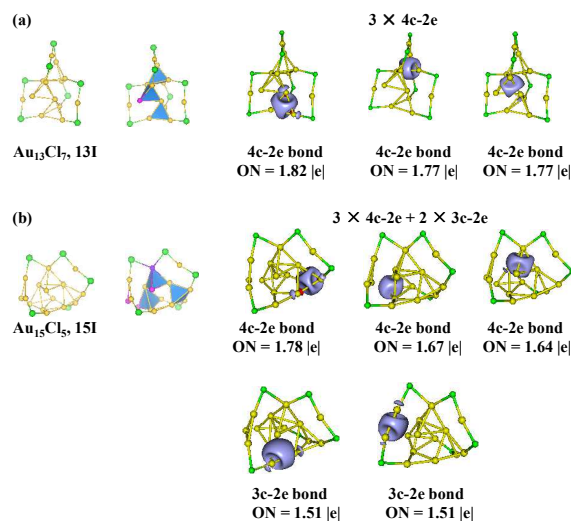


**Fig. 5** Structures, superatom-network models and AdNDP localized natural bonding orbitals of (a)  $\text{Au}_{13}\text{Cl}_7$  and (b)  $\text{Au}_{15}\text{Cl}_5$ . Au, yellow, Cl, green.

## 2.1 $\text{Au}_{11}\text{Cl}_9$ - $\text{Au}_{15}\text{Cl}_5$

**$\text{Au}_{11}\text{Cl}_9$ .**  $\text{Au}_{11}\text{Cl}_9$  is a 2e compound according to the superatom model.<sup>32</sup> The lowest-lying isomer (11I) contains one  $\text{Au}_5$  rectangular pyramid core protected by three  $-\text{Cl}-(\text{AuCl})_2-$  staple motifs. Chemical bonding analysis given by AdNDP reveals a  $5c-2e$  bond with occupancy number (ON) = 1.84 |e| (Fig. 3a). Such an  $\text{Au}_5$  2e-superatom has not been viewed in the experimentally produced Au-SR clusters. Moreover, there is one overprotected Au atom (labeled in purple and linked by two Cl) in the  $\text{Au}_5$  core, which is also not viewed in experiments.

Note that the tetrahedral  $\text{Au}_4$  core has been theoretically predicted for small nanoparticles, such as in  $\text{Au}_{10}(\text{SR})_8$  and  $\text{Au}_8(\text{SR})_6$ .<sup>34, 35</sup> The corresponding Au-Cl isomer is 11IV (0.29 eV higher in energy than 11I), which also has an  $\text{Au}_4$  core protected by one  $-\text{Cl}-(\text{AuCl})_3-$  and one  $-\text{Cl}-(\text{AuCl})_4-$  motifs. AdNDP analysis confirms the  $4c-2e$  bond with ON = 1.77 |e| (Fig. 3b).

The trigonal bipyramid  $\text{Au}_5$  superatom is also viewed in 11V protected by three  $-\text{Cl}-(\text{AuCl})_2-$  motifs, which is 0.37 eV higher in energy than 11I. AdNDP chemical bonding analysis confirms the  $5c-2e$  bond with ON = 1.87 |e| (Fig. 3c).

**$\text{Au}_{12}\text{Cl}_8$ .**  $\text{Au}_{12}\text{Cl}_8$  is a 4e compound. The low-lying isomers follow the SAN ( $2 \times 2e$ ) model in electronic structure. Here we discuss the first four isomers 12I-IV with different SAN styles. Both 12I and 12II consist of a network of two non-conjugated tetrahedral  $\text{Au}_4$  superatoms. AdNDP analysis reveals two  $4c-2e$  bonds in 12I with ON = 1.76 |e| and 1.84 |e|, respectively, and the ONs in 12II are both 1.77 |e|. This binding pattern is in accordance with the experimentally synthesized 4e compounds  $\text{Au}_{18}(\text{SR})_{14}$ ,  $\text{Au}_{20}(\text{SR})_{16}$ ,  $\text{Au}_{24}(\text{SR})_{20}$  and  $\text{Au}_{24}(\text{SeR})_{20}$  clusters.<sup>6, 72-75</sup>

12III also consists of a network of two non-conjugated  $\text{Au}_4$  cores protected by four  $-\text{Cl}-\text{Au}-\text{Cl}-$  motifs. AdNDP analysis

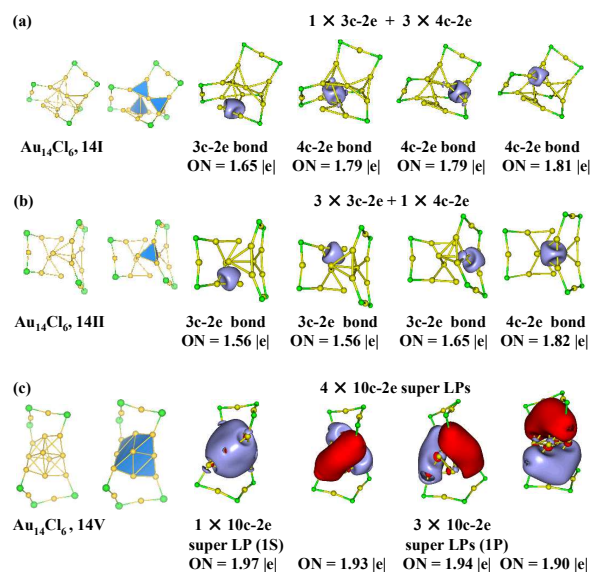


**Fig. 6** Structures, superatom models and AdNDP localized natural bonding orbitals of the three isomers of  $Au_{14}Cl_6$ : (a) 14I, (b) 14II and (c) 14V. Au, yellow, Cl, green.

reveals two 4c-2e bonds with ON = 1.61|e|. However, there are two overprotected Au atoms (labeled in purple) and two naked Au atoms (marked in magenta) in the two  $Au_4$  cores (Fig. 4c).

12IV has a unique vertex-sharing bitetrahedral  $Au_7$  core which is composed of two conjugated  $Au_4$  cores, ON = 1.83 |e| (Fig. 4d). Such a vertex-sharing  $Au_7$  kernel is consistent with the experimentally determined structure of  $Au_{20}(SR)_{16}$  cluster.<sup>73</sup>

**$Au_{13}Cl_7$ .** 13I is a 6e compound, and the cores of which can be viewed as a SAN ( $3 \times 2e$ ) of three conjugated vertex-sharing tetrahedral  $Au_4$  superatoms. Chemical bonding analysis given by AdNDP reveals three conjugated 4c-2e bonds with ON = 1.77-1.82 |e| (Fig. 5a). There is one naked Au atom (marked with magenta) in one  $Au_4$  superatom. The  $Au_4$  vertex-sharing conformation has been revealed in 12e  $Au_{36}(SR)_{24}$  cluster.<sup>76</sup>

**$Au_{14}Cl_6$ .**  $Au_{14}Cl_6$  cluster is a 8e compound according to the superatom model. As shown in Fig. 6a, 14I can be viewed as a  $4 \times 2e$  SAN of one  $Au_3$  superatom and three  $Au_4$  superatoms stapled by two -Cl units and two -Cl-Au-Cl- units. In addition, the superatoms are vertex-sharing. The ON of the 3c-2e bond is 1.65 |e|, and those of the 4c-2e bonds are 1.79-1.81 |e|. Such a 3c-2e superatom is not viewed in experimentally produced Au-SR clusters. 14II is also a  $4 \times 2e$  SAN, which consists of three  $Au_3$  superatoms and one  $Au_4$  superatom stapled by three -Cl-Au-Cl- units and lies 0.49 eV higher in energy than 14I. The experimentally produced  $Au_{28}(SR)_{20}$  cluster is a  $4 \times 2e$  SAN with four tetrahedral  $Au_4$  2e-superatoms in electronic structure.<sup>77, 78</sup>

14V is a 8e-superatom, which consists of one tetrahedral  $Au_{10}$  core stapled by two -Cl-(AuCl)<sub>2</sub>- units. AdNDP analysis reveals  $1S^2 1P^6$  superatom orbitals in the tetrahedron (Fig. 6c). It is worth noting that 14V lies 0.97 eV higher in energy than 14I, indicating that  $4 \times 2e$  SAN is favoured more than 8e-superatom for Au-Cl system.

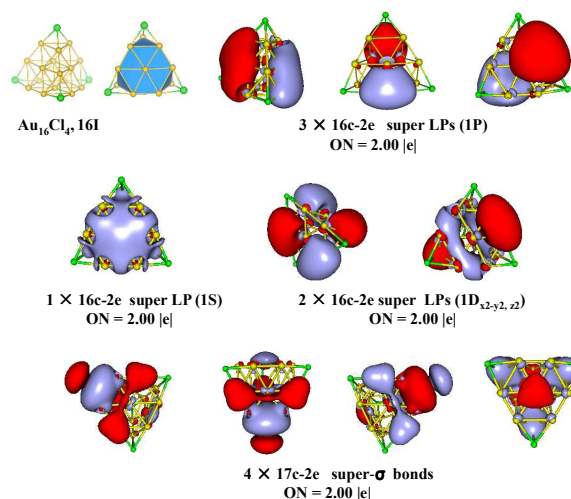


**Fig. 7** Structure, superatomic molecule model and AdNDP localized natural bonding orbitals of  $Au_{16}Cl_4$ , 16I. Au, yellow, Cl, green.

**$Au_{15}Cl_5$ .** 15I is a 10e compound, which can be viewed as a SAN of three  $Au_4$  superatoms and two  $Au_3$  superatoms stapled by three -Cl units and one -Cl-Au-Cl- unit (Fig. 5b). AdNDP reveals two 3c-2e bonds and three 4c-2e bonds. There are three naked Au atoms (marked with magenta) and one overprotected Au atom (labeled in purple) in 15I. The Au cores in 15I are not well protected by the staple motifs due to the lack of Cl, and it is not stable as shown in the SPD curve.

## 2.2 $Au_{16}Cl_4$ - $Au_{20}$

It is well known that the global minimum structure of  $Au_{20}$  is a pyramid.<sup>20, 79, 80</sup> The calculated HOMO-LUMO gap is 1.91 eV, in agreement with the experimental value (1.77 eV).<sup>20</sup> According to our extensive global search, the global minimum structures of  $Au_{16}Cl_4$ ,  $Au_{17}Cl_3$ ,  $Au_{18}Cl_2$  and  $Au_{19}Cl$  all base on the  $Au_{20}$  pyramid.

16I is a vertex-replaced  $Au_{20}$  pyramid, where the four Au on the vertexes are replaced by Cl. Similarly, 17I, 18I and 19I can be regarded as the three, two and one Au on the vertexes substituted by Cl, respectively.

The full-filled 5d electrons in Au ( $5d^{10}6s^1$ ) atoms of 16I, 17I, 18I, 19I and 20I clusters are mainly localized as LPs and  $6s^1$  are free valence electrons. Recently, our group has investigated the chemical bonding in pyramid  $Au_{20}$  using the SVB model.<sup>43</sup>  $Au_{20}$  can be viewed as a superatomic molecule, in which the superatomic 16c-16e core (T) is in  $D^3S$  hybridization bonded with four vertical Au atoms for molecule-like ( $TAu_4$ ) electronic shell-closure. Fig. 7 plots the AdNDP chemical bonding of 16I. As shown in the figure, there are six 16c-2e super LPs of T (super 1S, 1P and  $1D_{x^2-y^2, z^2}$ ) and four 17c-2e T-Cl super  $\sigma$ -bonds in 16I. Thus, similar to  $Au_{20}$ , 16I can also be viewed as a superatomic molecule with four T-Cl superatom-atom bonds. Similarly, 17I, 18I and 19I are also superatomic molecules (see Fig. S3†, Fig. S4† and Fig. S5†). Moreover, the linearity of the SPD curve at  $x = 16-20$  indicates that the five global minimum structures are equally competitive based on the composition.

### 2.3 Au<sub>9</sub>Cl<sub>11</sub>- Au<sub>5</sub>Cl<sub>5</sub>

When  $x$  ranges from 9 to 5, the clusters are Cl-rich, and the 5d electrons of Au atoms participate in bonding, resulting in high multiplicities (Fig. 1).

**Au<sub>9</sub>Cl<sub>11</sub>.** 9I is in C<sub>2</sub> symmetry with a pentamer ring inserting into a hexamer ring, and the multiplicity is 3. The oxidation state of the two Au atoms on the two crossing points are +2.

**Au<sub>8</sub>Cl<sub>12</sub>.** 8I is a rather open structure in singlet state with two crossing points. 8IV is a helix isomer (triplet state), in which the oxidation state of the four Au atoms on the four crossing over points are +2.

**Au<sub>7</sub>Cl<sub>13</sub>.** 7I is a triplet C<sub>2</sub> structure, which has four intersection points. 7II, 7III and 7IV are in high multiplicities (3, 5 and 7), lying much higher in energy than 7I.

**Au<sub>6</sub>Cl<sub>14</sub>.** 6I is a triplet C<sub>1</sub> structure and has six crossover points. 6IV and 6V are in high multiplicities (7 and 5), and each consisting of a quasi-cube unit and a Cl<sub>2</sub> molecule.

**Au<sub>5</sub>Cl<sub>15</sub>.** 5I is a triplet C<sub>1</sub> structure, which has two intersection points and one separate Cl<sub>2</sub> molecule.

### 3. Discussion

In this work, we replace -SR, -SeR, -PR<sub>2</sub> with -Cl to investigate the energy landscape of the Au-L system. Jiang et al. have performed a DFT work of Au<sub>25</sub>X<sub>18</sub><sup>-</sup> (wherein X = F, Cl, Br and I) and found that the electronic structure of Au<sub>25</sub>Cl<sub>18</sub><sup>-</sup> is almost identical to that of Au<sub>25</sub>(SR)<sub>18</sub><sup>-</sup>.<sup>33</sup> Moreover, there is high similarity between the frameworks of Au-S and Au-X systems. The structural patterns of Au-SR and Au-Cl systems are similar, indicating that the replacement of L by -Cl in Au-L systems is reasonable. This points to a way to predict the structures of Au-SR clusters by exploring Au-X clusters. Computationally, this greatly simplifies the process since the optimization of Au-Cl system is much easier than that of Au-SR system for the former contain less elements.

Pei et al. reviewed the structural evolution of Au-SR clusters.<sup>81</sup> The tetrahedral Au<sub>4</sub>-units in Au<sub>24</sub>(SR)<sub>20</sub> as well as the Au<sub>6</sub> and Au<sub>8</sub> cores in Au<sub>12</sub>(SR)<sub>9</sub><sup>+</sup> and Au<sub>18</sub>(SR)<sub>14</sub> support the existence of a major structural transition for Au-SR clusters at relatively small sizes. Moreover, the Au<sub>11</sub>-core in Au<sub>19</sub>(SR)<sub>13</sub> and Au<sub>23</sub>-core in Au<sub>38</sub>(SR)<sub>24</sub> clusters can be viewed as a manifestation of the structural evolution of Au cores from small-to-medium sizes. It is worth noting that the cluster sizes in the review are relatively big with respect to our study system.

There are corresponding structures to most of the experimentally synthesized and theoretically predicted Au-L nanoclusters in our SPD. Au<sub>11</sub>Cl<sub>9</sub> cluster, which has an Au<sub>4</sub> core protected by staple motifs, corresponds to Au<sub>10</sub>(SR)<sub>8</sub> and Au<sub>8</sub>(SR)<sub>6</sub>.<sup>34, 35</sup> Au<sub>12</sub>Cl<sub>8</sub> cluster corresponds to the experimentally synthesized Au<sub>18</sub>(SR)<sub>14</sub>, Au<sub>20</sub>(SR)<sub>16</sub>, Au<sub>24</sub>(SR)<sub>20</sub> and Au<sub>24</sub>(SeR)<sub>20</sub> clusters.<sup>6, 72-75</sup> Au<sub>13</sub>Cl<sub>7</sub> follows the SAN (3 × 2e) model in electronic structure, and the cores of which favour the vertex-sharing conformation revealed in 12e compound Au<sub>36</sub>(SR)<sub>24</sub>.<sup>76</sup> Au<sub>14</sub>Cl<sub>6</sub> follows 4 × 2e SAN, which are associated with the experimentally synthesized Au<sub>28</sub>(SR)<sub>20</sub> cluster in electronic structure.<sup>77, 78</sup> Au<sub>15</sub>Cl<sub>5</sub> follows 5 × 2e SAN. At  $x = 16-20$ , the global minimum structures of the Au-Cl

system are all pyramidal structures. There are also differences between the electronic structures of Au-SR and Au-Cl systems. The Au<sub>3</sub> and Au<sub>5</sub> superatoms found in Au-Cl system are not experimentally viewed in Au-SR system. Of note, several structures of the Au-Cl system are not reasonable, for example, Au<sub>5</sub>Cl<sub>15</sub> and Au<sub>15</sub>Cl<sub>5</sub>, which are Cl-rich and Au-rich clusters, respectively. This may be due to the restriction of  $x + y = 20$ , which results in the lack of Au atoms and Cl atoms in Au<sub>5</sub>Cl<sub>15</sub> and Au<sub>15</sub>Cl<sub>5</sub> clusters, respectively. There are naked Au atoms in gold cores of Au<sub>15</sub>Cl<sub>5</sub> due to the lack of Cl atoms in the structure. Our investigation gives all the possible chemical bonding patterns for the studied Au-Cl system.

From our work, we can see that when we substitute -SR, -SeR, -PR<sub>2</sub> ligands with -Cl in Au-L system, the Au-Cl clusters still maintain the magic number series, and present gold cores and similar staple motifs. The great diversity of Au-L systems indicates that gold nanoparticles have their own universe in chemistry, and our work gives an overall perspective to this universe.

### V. Conclusions

In present work, the Au-Cl binary system is taken as a test case to investigate the EL of Au-L system using the method combining GA with DFT. The sum of Au and Cl atoms are set to 20, in which the two magic number clusters Au<sub>10</sub>(SR)<sub>10</sub> and Au<sub>20</sub> are contained. We find a diverse set of global minimum structures and low-lying isomers for the system. The SAN and SVB models are used to characterize the bonding patterns. The Au-Cl binary system shows great diversity and flexibility in electronic and geometric structures. This work gives a direct and overall view of the structural evolution of the Au-Cl system at relatively small size. The electronic structures of the Au-Cl clusters evolve from structures with high multiplicities to catenane conformation, to structures containing superatoms, superatom network and finally to superatomic molecules. There are corresponding structures to most of the experimentally synthesized and theoretically predicted Au-L nanoclusters in our SPD. This work indicates that the Au-L systems are of great diversity.

These insights are expected to offer some new perspectives in terms of structural evolution in Au-L nanoclusters. We believe that our work gives an overall and direct view of the universe of Au-L system.

### Acknowledgements

This work is supported by the National Natural Science Foundation of China (21273008). The calculations are carried out on the High-Performance Computing Centre of Anhui University.

### References

1. J. Jung, S. Kang and Y. K. Han, *Nanoscale*, 2012, **4**, 4206-4210.
2. M. Z. Zhu, C. M. Aikens, M. P. Hendrich, R. Gupta, H. F. Qian, G. C. Schatz and R. C. Jin, *J. Am. Chem. Soc.*, 2009, **131**, 2490-2492.

3. H. T. Liu, X. G. Xiong, P. D. Dau, Y. L. Wang, J. Li and L. S. Wang, *Chem. Sci.*, 2011, **2**, 2101-2108.
4. P. Pyykkö, *Angew. Chem. Int. Ed.*, 2004, **43**, 4412-4456.
5. W. Lu, K. T. Chan, S. X. Wu, Y. Chen and C. M. Che, *Chem. Sci.*, 2012, **3**, 752-755.
6. Y. Negishi, K. Nobusada and T. Tsukuda, *J. Am. Chem. Soc.*, 2005, **127**, 5261-5270.
7. M. P. Johansson, A. Lechtken, D. Schooss, M. M. Kappes and F. Furche, *Phys. Rev. A*, 2008, **77**, 053202.
8. A. Lechtken, C. Neiss, M. M. Kappes and D. Schooss, *Phys. Chem. Chem. Phys.*, 2009, **11**, 4344-4350.
9. W. Huang, S. Bulusu, R. Pal, X. C. Zeng and L. S. Wang, *ACS nano*, 2009, **3**, 1225-1230.
10. L. Ferrighi, B. Hammer and G. K. Madsen, *J. Am. Chem. Soc.*, 2009, **131**, 10605-10609.
11. X. P. Xing, B. Yoon, U. Landman and J. H. Parks, *Phys. Rev. B*, 2006, **74**, 165423.
12. S. Bulusu and X. C. Zeng, *J. Chem. Phys.*, 2006, **125**, 154303.
13. M. Walter and H. Häkkinen, *Phys. Chem. Chem. Phys.*, 2006, **8**, 5407-5411.
14. S. Bulusu, X. Li, L. S. Wang and X. C. Zeng, *Proc. Natl. Acad. Sci. USA*, 2006, **103**, 8326-8330.
15. X. Gu, S. Bulusu, X. Li, X. C. Zeng, J. Li, X. G. Gong and L. S. Wang, *J. Phys. Chem. C*, 2007, **111**, 8228-8232.
16. M. Ji, X. Gu, X. Li, X. G. Gong, J. Li and L. S. Wang, *Angew. Chem. Int. Ed.*, 2005, **117**, 7281-7285.
17. A. Lechtken, D. Schooss, J. R. Stairs, M. N. Blom, F. Furche, N. Morgner, O. Kostko, B. von Issendorff and M. M. Kappes, *Angew. Chem. Int. Ed.*, 2007, **46**, 2944-2948.
18. B. Schaefer, R. Pal, N. S. Khetrapal, M. Amsler, A. Sadeghi, V. Blum, X. C. Zeng, S. Goedecker and L. S. Wang, *ACS Nano*, 2014, **8**, 7413-7422.
19. N. Shao, W. Huang, W. N. Mei, L. S. Wang, Q. Wu and X. C. Zeng, *J. Phys. Chem. C*, 2014, **118**, 6887-6892.
20. J. Li, X. Li, H. J. Zhai and L. S. Wang, *Science*, 2003, **299**, 864-867.
21. P. Gruene, D. M. Rayner, B. Redlich, A. F. van der Meer, J. T. Lyon, G. Meijer and A. Fielicke, *Science*, 2008, **321**, 674-676.
22. H. F. Zhang, M. Stender, R. Zhang, C. Wang, J. Li and L. S. Wang, *J. Phys. Chem. B*, 2004, **108**, 12259-12263.
23. P. D. Jadzinsky, G. Calero, C. J. Ackerson, D. A. Bushnell and R. D. Kornberg, *Science*, 2007, **318**, 430-433.
24. M. Z. Zhu, C. M. Aikens, F. J. Hollander, G. C. Schatz and R. C. Jin, *J. Am. Chem. Soc.*, 2008, **130**, 5883-5885.
25. H. F. Qian, Y. Zhu and R. C. Jin, *ACS nano*, 2009, **3**, 3795-3803.
26. M. Z. Zhu, H. F. Qian and R. C. Jin, *J. Phys. Chem. Lett.*, 2010, **1**, 1003-1007.
27. X. K. Wan, Z. W. Lin and Q. M. Wang, *J. Am. Chem. Soc.*, 2012, **134**, 14750-14752.
28. T. D. Green, C. Y. Yi, C. J. Zeng, R. C. Jin, S. McGill and K. L. Knappenberger, *J. Phys. Chem. A*, 2014, **118**, 10611-10321.
29. D. E. Jiang, S. H. Overbury and S. Dai, *J. Am. Chem. Soc.*, 2013, **135**, 8786-8789.
30. M. Walter, M. Moseler, R. L. Whetten and H. Häkkinen, *Chem. Sci.*, 2011, **2**, 1583-1587.
31. P. R. Nimmala, S. Knoppe, V. R. Jupally, J. H. Delcamp, C. M. Aikens and A. Dass, *J. Phys. Chem. B*, 2014, **118**, 14157-14167.
32. M. Walter, J. Akola, O. Lopez-Acevedo, P. D. Jadzinsky, G. Calero, C. J. Ackerson, R. L. Whetten, H. Grönbeck and H. Häkkinen, *Proc. Natl. Acad. Sci.*, 2008, **105**, 9157-9162.
33. D. E. Jiang and M. Walter, *Nanoscale*, 2012, **4**, 4234-4239.
34. D. E. Jiang, W. Chen, R. L. Whetten and Z. F. Chen, *J. Phys. Chem. C*, 2009, **113**, 16983-16987.
35. D. E. Jiang, R. L. Whetten, W. D. Luo and S. Dai, *J. Phys. Chem. C*, 2009, **113**, 17291-17295.
36. D. E. Jiang, M. Walter and J. Akola, *J. Phys. Chem. C*, 2010, **114**, 15883-15889.
37. Y. Gao, N. Shao and X. C. Zeng, *ACS nano*, 2008, **2**, 1497-1503.
38. Y. Gao, *J. Phys. Chem. C*, 2013, **117**, 8983-8988.
39. L. J. Cheng, Y. Yuan, X. Z. Zhang and J. L. Yang, *Angew. Chem. Int. Ed.*, 2013, **52**, 9035-9039.
40. Y. Pei, S. S. Lin, J. C. Su and C. Y. Liu, *J. Am. Chem. Soc.*, 2013, **135**, 19060-19063.
41. L. J. Cheng and J. L. Yang, *J. Chem. Phys.*, 2013, **138**, 141101.
42. L. J. Cheng, C. D. Ren, X. Z. Zhang and J. L. Yang, *Nanoscale*, 2013, **5**, 1475-1478.
43. L. J. Cheng, X. Z. Zhang, B. K. Jin and J. L. Yang, *Nanoscale*, 2014, **6**, 12440-12444.
44. Y. Yuan, L. J. Cheng and J. L. Yang, *J. Phys. Chem. C*, 2013, **117**, 13276-13282.
45. N. Shao, Y. Pei, Y. Gao and X. C. Zeng, *J. Phys. Chem. A*, 2009, **113**, 629-632.
46. A. Tlaluice and I. L. Garzón, *Phys. Chem. Chem. Phys.*, 2012, **14**, 3737-3740.
47. S. L. Christensen, M. A. MacDonald, A. Chatt, P. Zhang, H. F. Qian and R. C. Jin, *J. Phys. Chem. C*, 2012, **116**, 26932-26937.
48. A. Das, C. Liu, C. J. Zeng, G. Li, T. Li, N. L. Rosi and R. C. Jin, *J. Phys. Chem. A*, 2014, **118**, 8264-8269.
49. B. Assadollahzadeh and P. Schwerdtfeger, *J. Chem. Phys.*, 2009, **131**, 064306.
50. A. Dass, P. R. Nimmala, V. R. Jupally and N. Kothalawala, *Nanoscale*, 2013, **5**, 12082-12085.
51. W. Fa, C. F. Luo and J. M. Dong, *Phys. Rev. B*, 2005, **72**, 205428.
52. Y. Li, G. Galli and F. Gygi, *ACS nano*, 2008, **2**, 1896-1902.
53. O. Lopez-Acevedo, J. Akola, R. L. Whetten, H. Grönbeck and H. Häkkinen, *J. Phys. Chem. C*, 2009, **113**, 5035-5038.
54. R. Ferrando, J. Jellinek and R. L. Johnston, *Chem. Rev.*, 2008, **108**, 845-910.
55. L. Ren, L. J. Cheng, Y. Feng and X. M. Wang, *J. Chem. Phys.*, 2012, **137**, 014309.
56. L. J. Cheng, *J. Chem. Phys.*, 2012, **136**, 104301.
57. L. F. Li and L. J. Cheng, *J. Chem. Phys.*, 2013, **138**, 094312.
58. Y. Yuan and L. Cheng, *J. Chem. Phys.*, 2012, **137**, 044308.
59. D. M. Deaven and K. M. Ho, *Phys. Rev. Lett.*, 1995, **75**, 288-291.



## ARTICLE

## Physical Chemistry Chemical Physics

60. R. L. Johnston, *Dalton Trans.*, 2003, 4193-4207.
61. A. Shayeghi, D. Götz, J. Davis, R. Schaefer and R. L. Johnston, *Phys. Chem. Chem. Phys.*, 2015, **17**, 2104-2112.
62. M. J. Frisch, H. B. Schlegel, G. E. Scuseria, M. A. Robb, J. R. Cheeseman, G. Scalmani, V. Barone, B. Mennucci, G. A. Petersson, H. Nakatsuji, M. Caricato, X. Li, H. P. Hratchian, A. F. Izmaylov, J. Bloino, G. Zheng, J. L. Sonnenberg, M. Hada, M. Ehara, K. Toyota, R. Fukuda, J. Hasegawa, M. Ishida, T. Nakajima, Y. Honda, O. Kitao, H. Nakai, T. Vreven, J. A. Montgomery, J. E. P. Jr., F. Ogliaro, M. Bearpark, J. J. Heyd, E. Brothers, K. N. Kudin, V. N. Staroverov, T. Keith, R. Kobayashi, J. Normand, K. Raghavachari, A. Rendell, J. C. Burant, S. S. Iyengar, J. Tomasi, M. Cossi, N. Rega, J. M. Millam, M. Klene, J. E. Knox, J. B. Cross, V. Bakken, C. Adamo, J. Jaramillo, R. Gomperts, R. E. Stratmann, O. Yazyev, A. J. Austin, R. Cammi, C. Pomelli, J. W. Ochterski, R. L. Martin, K. Morokuma, V. G. Zakrzewski, G. A. Voth, P. Salvador, J. J. Dannenberg, S. Dapprich, A. D. Daniels, O. Farkas, J. B. Foresman, J. V. Ortiz, J. Cioslowski and D. J. Fox, *Gaussian, Inc., Wallingford, CT*, 2010.
63. K. L. Schuchardt, B. T. Didier, T. Elsethagen, L. S. Sun, V. Gurumoorathi, J. Chase, J. Li and T. L. Windus, *J. Chem. Inf. Model.*, 2007, **47**, 1045-1052.
64. F. Weigend and R. Ahlrichs, *Phys. Chem. Chem. Phys.*, 2005, **7**, 3297-3305.
65. J. Tao, J. P. Perdew, V. N. Staroverov and G. E. Scuseria, *Phys. Rev. Lett.*, 2003, **91**, 146401.
66. N. Version, Weinhold, 1995.
67. D. Y. Zubarev and A. I. Boldyrev, *Phys. Chem. Chem. Phys.*, 2008, **10**, 5207-5217.
68. U. Varetto, *Swiss National Supercomputing Centre: Manno, Switzerland*, 2009.
69. K. P. Huber and G. Herzberg, *Constants of diatomic molecules*, Springer, 1979.
70. Y. Pei, R. Pal, C. Liu, Y. Gao, Z. Zhang and X. C. Zeng, *J. Am. Chem. Soc.*, 2012, **134**, 3015-3024.
71. S. S. Y. Chui, R. Chen and C. M. Che, *Angew. Chem.*, 2006, **118**, 1651-1654.
72. M. Z. Zhu, H. F. Qian and R. C. Jin, *J. Am. Chem. Soc.*, 2009, **131**, 7220-7221.
73. C. J. Zeng, C. Liu, Y. X. Chen, N. L. Rosi and R. C. Jin, *J. Am. Chem. Soc.*, 2014, **136**, 11922-11925.
74. Y. B. Song, S. X. Wang, J. Zhang, X. Kang, S. Chen, P. Li, H. T. Sheng and M. Z. Zhu, *J. Am. Chem. Soc.*, 2014, **136**, 2963-2965.
75. A. Das, T. Li, G. Li, K. Nobusada, C. J. Zeng, N. L. Rosi and R. C. Jin, *Nanoscale*, 2014, **6**, 6458-6462.
76. D. M. Chevrier, A. Chatt, P. Zhang, C. J. Zeng and R. C. Jin, *J. Phys. Chem. Lett.*, 2013, **4**, 3186-3191.
77. C. J. Zeng, T. Li, A. Das, N. L. Rosi and R. C. Jin, *J. Am. Chem. Soc.*, 2013, **135**, 10011-10013.
78. S. Knoppe, S. Malola, L. Lehtovaara, T. Bürgi and H. Häkkinen, *J. Phys. Chem. A*, 2013, **117**, 10526-10533.
79. J. L. Wang, G. H. Wang and J. J. Zhao, *Chem. Phys. Lett.*, 2003, **380**, 716-720.
80. R. B. King, Z. F. Chen and P. v. R. Schleyer, *Inorg. Chem.*, 2004, **43**, 4564-4566.
81. Y. Pei and X. C. Zeng, *Nanoscale*, 2012, **4**, 4054-4072.

**Table of Contents Entry**

Structural phase diagram (SPD) of  $\text{Au}_x\text{Cl}_y$  ( $x + y = 20$ ) clusters.

